

HAPNet: Toward Superior RGB-Thermal Scene Parsing via Hybrid, Asymmetric, and Progressive Heterogeneous Feature Fusion

Jiahang Li,^{id} *Graduate Student Member, IEEE*, Peng Yun^{id},

Qijun Chen^{id} *Senior Member, IEEE*, Rui Fan^{id} *Senior Member, IEEE*

Abstract—Data-fusion networks have shown significant promise for RGB-thermal scene parsing. However, the majority of existing studies have relied on symmetric duplex encoders for heterogeneous feature extraction and fusion, paying inadequate attention to the inherent differences between RGB and thermal modalities. Recent progress in vision foundation models (VFMs) trained through self-supervision on vast amounts of unlabeled data has proven their ability to extract informative, general-purpose features. However, this potential has yet to be fully leveraged in the domain. In this study, we take one step toward this new research area by exploring a feasible strategy to fully exploit VFM features for RGB-thermal scene parsing. Specifically, we delve deeper into the unique characteristics of RGB and thermal modalities, thereby designing a hybrid, asymmetric encoder that incorporates both a VFM and a convolutional neural network. This design allows for more effective extraction of complementary heterogeneous features, which are subsequently fused in a dual-path, progressive manner. Moreover, we introduce an auxiliary task to further enrich the local semantics of the fused features, thereby improving the overall performance of RGB-thermal scene parsing. Our proposed HAPNet, equipped with all these components, demonstrates superior performance compared to all other state-of-the-art RGB-thermal scene parsing networks, achieving top ranks across three widely used public RGB-thermal scene parsing datasets. We believe this new paradigm has opened up new opportunities for future developments in data-fusion scene parsing approaches.

Index Terms—data-fusion, thermal, scene parsing, heterogeneous feature, vision foundation model.

I. INTRODUCTION

A. Background

UNITY in diversity strengthens perception. RGB-thermal (often abbreviated as RGB-T) scene parsing has emerged as a crucial feature in autonomous vehicles and mobile robots [1]. RGB images capture visible light, while thermal images capture heat signatures [2]. The fusion of these two modalities of data, especially during the feature encoding stage, has been proven to dramatically enhance the reliability and robustness of scene parsing [3]–[5]. Nevertheless, current data-fusion approaches [6]–[11] generally employ duplex [12]–[14] encoders (two identical pre-trained hierarchical backbone networks with independent trainable parameters) to indiscriminately extract heterogeneous features from the RGB-T data, limiting their ability to fully exploit the advantages of both data modalities [15]. Therefore, this study aims to explore a more ingenious and effective strategy for heterogeneous feature extraction

and fusion, with a specific focus on leveraging VFMs, as exemplified by BEiT series [16], [17] and DINOv2 [18], which have garnered considerable attention in recent computer vision research endeavors.

B. Existing Challenges and Motivation

The backbone networks in duplex encoders are commonly pre-trained on the ImageNet database [19] (containing millions of annotated natural images) through fully supervised learning. Although the ImageNet database has enabled these networks to closely approximate real-world data distributions, its limited dataset size restricts these networks from fully exploiting the vast amount of unlabeled data available worldwide [16]. Unfortunately, designing encoders based on VFMs, pre-trained in a self/un-supervised manner on extensive unlabeled data, for heterogeneous feature extraction remains largely unexplored in the domain of RGB-T scene parsing.

Additionally, while symmetric duplex encoders [10], [20], [21] are prevalently used, they may not be the optimal architectures for heterogeneous feature extraction. This limitation arises from the substantial inherent modality difference [22] between the RGB and thermal images, as well as the unique advantages provided by vision Transformers (ViTs) and convolutional neural networks (CNNs). RGB images, rich in global semantic cues [23], are well-suited for learning through ViTs, while both RGB and thermal images provide gradient-related details (local semantics) [9], [24], which can be more effectively learned through CNNs. Therefore, developing a novel asymmetric duplex encoder, with ViT and CNN employed separately in each branch, for RGB-T scene parsing, stands as an underexplored area of research deserving greater attention.

Moreover, the heterogeneous feature fusion strategy is of considerable importance in RGB-T scene parsing. The simplistic and indiscriminate strategies used in prior arts [4], [5], [21], [25] often cause conflicting feature representations and erroneous scene parsing results [15]. Taking MFNet [5] as an instance, its feature fusion relies solely on the element-wise concatenation of the heterogeneous features extracted from the duplex encoders at their final stage, treating the features from both modalities equally in the decoder’s input. Such a hard-coded feature fusion strategy overlooks the inherent differences in RGB-T feature characteristics and their respective reliability [9], resulting in unsatisfactory performance,

particularly under poor illumination conditions. Therefore, another motivation for this article is to design an effective strategy for heterogeneous feature fusion, especially when these features are extracted from different modalities using an asymmetric duplex encoder.

C. Contributions

To address the aforementioned limitations, we investigate the use of VFMs for RGB-T scene parsing, thereby unleashing the power of self-supervised pre-training on extensive unlabeled data. Given the inherent differences between RGB and thermal images, we first develop a cross-modal spatial prior descriptor (CSPD) based on a CNN to capture robust local spatial patterns from both RGB and thermal images. We then combine the CSPD with a VFM to construct a hybrid, asymmetric encoder, which fuses the heterogeneous features (global context extracted from RGB images and spatial prior captured from RGB-T data) using a progressive heterogeneous feature integrator (PHFI). This dual-path, progressive strategy enables deeper fusion of heterogeneous features. Additionally, we introduce an auxiliary task to implicitly enrich the local semantics of the fine-grained fused features, thereby further improving the overall performance of RGB-T scene parsing. Our proposed **Hybrid, Asymmetric, and Progressive Network (HAPNet)** achieves the top rankings across three public RGB-T scene parsing datasets.

In a nutshell, this study makes the following contributions:

- We investigate the potential of VFM for RGB-T scene parsing and propose an asymmetric encoder that enables VFMs to achieve effective heterogeneous feature fusion.
- By revisiting the inherent characteristics of RGB and thermal modalities, we design a hybrid, asymmetric encoder to fully exploit the strengths of both modalities.
- We propose an auxiliary task to further enrich the local semantics of the fine-grained fused features.
- Our proposed HAPNet achieves SoTA performance on three publicly available RGB-T scene parsing datasets, and demonstrates promising generalizability for RGB-HHA scene parsing.

D. Outline

The remainder of this article is structured as follows: Sect. II reviews related works. Sect. III details our proposed HAPNet. Sect. IV compares HAPNet with other SoTA methods and presents the ablation study results. Finally, Sect. V concludes this article and discusses possible future work.

II. RELATED WORK

A. Single-Modal Scene Parsing

The advent of the fully convolutional network (FCN) [26] catalyzed a wave of research on CNN-based scene parsing networks, which typically utilize convolutions for pixel-wise classification and explore various modules and architectures to enhance overall performance. For instance, the DeepLab series [27], [28] leverages atrous spatial pyramid pooling to capture multi-scale context information, while the feature

pyramid network (FPN) [29] effectively fuses multi-scale features for robust dense prediction. Nonetheless, CNNs suffer from inherent limitations, *e.g.*, constrained receptive fields, which impede their effectiveness in comprehensively modeling global context.

Transformers [30], originally proposed for natural language processing, have revolutionized computer vision due to their capability to model long-range dependencies. As a representative example, segmentation Transformer (SETR) [31] introduces a ViT-based encoder for scene parsing, enabling long-range dependency modeling via self-attention mechanisms. Another approach, SegFormer [32], employs a hierarchical encoder to achieve multi-scale feature encoding within the Transformer framework, outperforming SETR in handling objects of varying sizes. Additionally, drawing upon earlier works [33], [34], the MaskFormer [35], [36] series formulates scene parsing as a mask classification problem. These networks utilize a Transformer decoder to refine object queries and generate pixel-level predictions. Given the impressive performance demonstrated by the MaskFormer architecture in dense prediction tasks, we adopt a similar network design for scene parsing in this study.

B. Data-Fusion Scene Parsing

The aforementioned single-modal networks often face challenges in handling complex scenes, especially under poor illumination and adverse weather conditions [2]. This is primarily because they rely solely on color and texture information present in RGB images [9]. Therefore, researchers have explored multi-modal/source data-fusion techniques (with duplex encoders) to overcome these limitations. MFNet [5] pioneers the use of duplex encoders for RGB-T scene parsing. It extracts heterogeneous features using two lightweight backbones and realizes feature fusion via element-wise concatenation, achieving a balance between speed and accuracy. Most subsequent studies generally employ element-wise summation to achieve heterogeneous feature fusion and focus more on encoder and decoder designs for improved performance. For example, RTFNet [4] introduces skip connections in the decoder to preserve clear boundaries and fine details. Similarly, FuseSeg [25] replaces the ResNet [12] backbone in RTFNet with the stronger DenseNet [37], enabling richer multi-scale feature extraction. Despite the improved performance achieved by these networks, the simplistic heterogeneous feature fusion strategies potentially limit their ability to fully exploit the complementary information present in RGB-T data.

To address this drawback, recent works [6]–[10], [20], [21] have resorted to more advanced, learnable feature fusion strategies. For instance, FEANet [21] and GMNet [9] introduce attention-based modules to dynamically select important heterogeneous features. Their subsequent research endeavor, CMX [8], employs average and max pooling operations along with the attention modules to recalibrate heterogeneous features at the spatial and channel dimensions. Similarly, CAINet [10] employs different attention modules to model global context and aggregate local semantics across various spatial scales of RGB-T feature maps. Moreover, the ABMDRNet

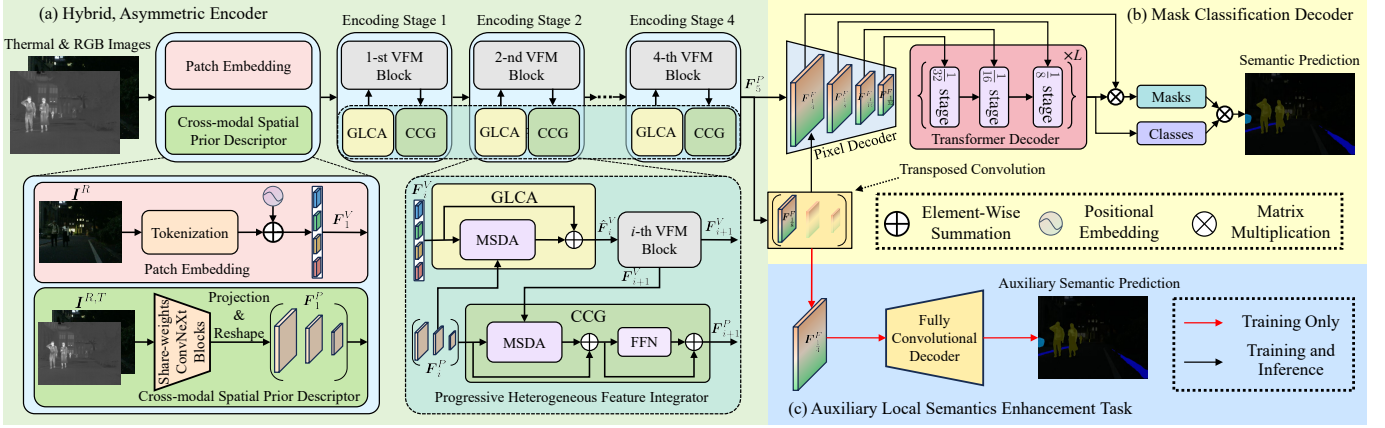


Fig. 1: An overview of our proposed HAPNet architecture.

series [6], [20] introduces novel modality-wise bridging-then-fusing frameworks, capable of reconstructing pseudo images of one modality using the features extracted from the other modality. This approach successfully reduces modality discrepancy and generates more discriminative fused features. Additionally, inspired by the masked auto-encoder (MAE) [38], CRM-RGBTseg [7] randomly corrupts fixed-size regions and subsequently recovers the corrupted regions from the other modality, preventing over-reliance on either modality. In this article, we employ a novel asymmetric duplex encoder to capture both local spatial priors and global context from the RGB-T data. These heterogeneous features are progressively fused for more robust scene parsing.

III. METHODOLOGY

This section details HAPNet, a hybrid, asymmetric network capable of progressively fusing heterogeneous features extracted from RGB-T data to perform scene parsing. As illustrated in Fig. 1, HAPNet comprises three key components:

- An asymmetric, hybrid encoder that extracts heterogeneous features from RGB-T data using a VFM (based on ViT) and a CSPD. In the meantime, these features are progressively fused via PHFI;
- A Transformer-based mask classification decoder that leverages the fused heterogeneous features to produce semantic predictions;
- An auxiliary task to further enhance the local semantics of fused heterogeneous features.

A. Overall Workflow

Unlike previous works that utilize symmetric duplex encoder structures, we innovatively introduce an asymmetric, hybrid architecture (based on both a Transformer-based VFM and a lightweight CNN). It effectively combines the complementary strengths of both modalities, thereby achieving deeper cross-modal feature fusion and further improving the overall performance. This is realized by dividing the ViT encoder into four blocks and inserting the PHFI to form four encoding stages. The RGB image $I^R \in \mathbb{R}^{H \times W \times 3}$ and its corresponding thermal image $I^T \in \mathbb{R}^{H \times W \times 3}$ are first

fed into the CSPD, extracting the cross-modal spatial prior $F_1^P \in \mathbb{R}^{(\sum_{i=2}^4 \frac{H \cdot W}{S_i^2}) \times D}$, which serves as one of the inputs to HAPNet, where $S_i = 2^{i+1}$ ($i \in [2, 4] \cap \mathbb{Z}$) denotes the corresponding stride number. Afterwards, I^R is tokenized to form the context feature $F_1^V \in \mathbb{R}^{\frac{H \cdot W}{16^2} \times D}$, which serves as the other input to HAPNet. F_1^V undergoes global context encoding in the following ViT blocks. F_1^V and F_1^P are then fused in a dual-path, progressive manner using the two key components of our developed PHFI: (1) the global-local context aggregator (GLCA) and (2) the complementary context generator (CCG). This design enables the RGB features to retain fine-grained local semantics while effectively capturing global context through the powerful VFM. Eventually, the fused features $\mathcal{F}^F = \{F_{\frac{1}{S_j}}^F \in \mathbb{R}^{\frac{H}{S_j} \times \frac{W}{S_j} \times D}\}$, where $S_j = 2^{j+1}$ ($j \in [1, 4] \cap \mathbb{Z}$) from the four encoding stages are obtained and then fed into the subsequent mask classification decoder to generate semantic predictions $M^P \in \mathbb{R}^{H \times W}$, which are also utilized by an auxiliary local semantics enhancement task during model training.

B. Hybrid, Asymmetric Encoder

1) *Encoding Pipeline*: We evenly divide I^R into non-overlapping patches (resolution: 16×16 pixels) and project them into D -dimensional tokens to form the RGB context feature F_1^V . In the i -th encoding stage, the input context features F_i^V and spatial prior F_i^P are first fused in the GLCA to generate local semantics-enhanced context feature $\hat{F}_i^V \in \mathbb{R}^{\frac{H \cdot W}{16^2} \times D}$. Subsequently, \hat{F}_i^V undergoes context encoding in the ViT block, generating the output F_{i+1}^V , which is then fed into the CCG to perform another fusion with F_i^P . This step complements spatial prior F_i^P with updated global context from F_{i+1}^V to generate F_{i+1}^P . By repeating such a dual-path feature fusion across four encoding stages, we obtain the fused spatial prior F_5^P , which is then recovered to its original three resolutions, forming $\{F_{\frac{1}{8}}^P, F_{\frac{1}{16}}^P, F_{\frac{1}{32}}^P\}$. A 2×2 transposed convolution is employed to directly create the $\frac{1}{4}$ -scale features $F_{\frac{1}{4}}^F$ from $F_{\frac{1}{8}}^P$. This design avoids the heavy computational overhead of the attention operations required for creating $F_{\frac{1}{4}}^F$. Finally, these fused features across four scales constitute \mathcal{F}^F ,

which is compatible with current SoTA scene parsing network architectures [35], [39].

Solely employing RGB images as the ViT input stems from our hypothesis that explicitly encoding thermal images using VFM may cause convergence issues and representation shift, as discussed in [40]. Furthermore, thermal data often has limited capability in capturing global context, as objects with similar geometries tend to have similar heat signatures. For example, distinguishing between a soccer ball and a basketball or between a cat and a dog is challenging in thermal images. We validate the effectiveness and superior performance of this hybrid, asymmetric network design through ablation studies in Sect. IV-E.

2) *Cross-modal Spatial Prior Descriptor*: Compared to Transformers [10], [41], CNNs have demonstrated superior performance in capturing local semantics, underscoring their significance in computer vision applications that necessitate clear object boundaries. ConvNeXt [14] have shown exceptional performance in capturing rich, robust visual features in comparison with other hierarchical CNN architectures such as ResNet [12] and its variants [42], as evidenced by recent endeavors using ConvNeXt for multi-modal scene parsing [43], [44]. Given these advantages, we employ basic ConvNeXt blocks to construct our CSPD. Furthermore, incorporating RGB data as a complementary input enables the CSPD to extract more comprehensive local spatial patterns than using thermal images alone. Consequently, we construct our CSPD using two identical, weight-sharing subnetworks, enabling efficient and effective extraction of cross-modal spatial priors from the RGB-T data.

Specifically, \mathbf{I}^R and \mathbf{I}^T are independently fed into a series of weight-sharing ConvNeXt blocks, generating multi-scale features $\mathcal{P}^R = \{\mathbf{P}_2^R, \mathbf{P}_3^R, \mathbf{P}_4^R\}$ and $\mathcal{P}^T = \{\mathbf{P}_2^T, \mathbf{P}_3^T, \mathbf{P}_4^T\}$, respectively, where $\mathbf{P}_i^{R,T} \in \mathbb{R}^{\frac{H}{S_i} \times \frac{W}{S_i} \times C_i}$ represents the features at i -th stage, C_i and $S_i = 2^{i+1}$ ($i \in [2, 4] \cap \mathbb{Z}$) denote the corresponding channel and stride numbers, respectively. We then combine \mathbf{P}_i^R and \mathbf{P}_i^T via element-wise summation, and reduce the results to D channels through 1×1 convolutions, yielding heterogeneous features $\mathcal{P}^H = \{\mathbf{P}_2^H, \mathbf{P}_3^H, \mathbf{P}_4^H\}$, where $\mathbf{P}_i^H \in \mathbb{R}^{\frac{H}{S_i} \times \frac{W}{S_i} \times D}$. The three-scale features are then flattened and concatenated to form the cross-modal spatial prior \mathbf{F}_1^P which is used for the following encoding stages. We present detailed ablation studies in Sect. IV-E to analyze the impact of different CSPD construction blocks and data input strategies on the overall performance.

3) *Progressive Heterogeneous Feature Integrator*: The GLCA and CCG, two attention-based components of our PHFI, are responsible for the dual-path feature fusion process before and after each ViT block, respectively. Given \mathbf{F}_i^V and \mathbf{F}_i^P of the i -th encoding block ($i \in [1, 4] \cap \mathbb{Z}$), we first feed them into the GLCA to obtain the local semantics-enhanced input $\hat{\mathbf{F}}_i^V$. Specifically, \mathbf{F}_i^V serves as the query, while \mathbf{F}_i^P acts as the key and value within the GLCA. This process can be formulated as follows:

$$\hat{\mathbf{F}}_i^V = \mathbf{F}_i^V + \kappa_i \text{MHA}(\text{LN}(\mathbf{F}_i^V), \text{LN}(\mathbf{F}_i^P)), \quad (1)$$

where $\text{MHA}(\cdot)$ represents the multi-head attention (MHA) operation (implemented based on multi-scale deformable at-

tention [36] to reduce computations) and $\text{LN}(\cdot)$ represents the layer normalization operation. Following common practices in attention modules such as [43], [45], we introduce a learnable coefficient κ_i to dynamically adjust the weight of the MHA, enabling flexible fusion of the local semantics-enhanced features into the VFM. After the i -th ViT block, the output feature maps \mathbf{F}_{i+1}^V with enriched global context are yielded. \mathbf{F}_{i+1}^V is then fed into the CCG to fuse its global context with the spatial prior \mathbf{F}_i^P . In this process, \mathbf{F}_i^P serves as the query, while \mathbf{F}_{i+1}^V acts as the keys and values to perform MHA within the CCG as follows:

$$\hat{\mathbf{F}}_i^P = \mathbf{F}_i^P + \text{MHA}(\text{LN}(\mathbf{F}_i^P), \text{LN}(\mathbf{F}_{i+1}^V)). \quad (2)$$

After the MHA operation, a feed-forward network (FFN) is applied to further process the fused features, resulting in the updated spatial prior \mathbf{F}_{i+1}^P , which have already incorporated rich local and global semantics and will be inputted to the next encoding stage.

C. Mask Classification Decoder

Following [36], our mask classification decoder consists of a pixel decoder and a Transformer decoder. The former improves the fused heterogeneous features $\{\mathbf{F}_{\frac{1}{8}}^F, \mathbf{F}_{\frac{1}{16}}^F, \mathbf{F}_{\frac{1}{32}}^F\}$, producing $\hat{\mathcal{F}}^P = \{\hat{\mathbf{F}}_{\frac{1}{8}}^P, \hat{\mathbf{F}}_{\frac{1}{16}}^P, \hat{\mathbf{F}}_{\frac{1}{32}}^P\}$, and generates the pixel embedding $\mathbf{E}^P \in \mathbb{R}^{C \times \frac{H}{4} \times \frac{W}{4}}$ from $\mathbf{F}_{\frac{1}{4}}^F$; The latter employs $\hat{\mathcal{F}}^P$ to refine a fixed size of queries, thus producing the mask embedding $\mathbf{E}^M \in \mathbb{R}^{Q \times C}$, where Q and C represent the numbers of queries and feature channels, respectively. \mathbf{E}^M is multiplied by \mathbf{E}^P to yield mask predictions $\mathbf{M}^M \in \mathbb{R}^{Q \times \frac{H}{4} \times \frac{W}{4}}$. By resizing \mathbf{M}^M and associating it with the class predictions $\mathbf{E}^C \in \mathbb{R}^{Q \times N}$ learned from queries, we obtain the semantic predictions \mathbf{M}^P , where N denotes the number of classes (including a ‘‘no object’’ class). Readers can refer to [36] for more details on this decoding process.

D. Auxiliary Local Semantics Enhancement Task

In our mask classification decoder, \mathbf{E}^P generated from $\mathbf{F}_{\frac{1}{4}}^F$ typically provides rich per-pixel semantics of the scene, while \mathbf{E}^M generated from the other three scales of features provides information on category-related cluster centers [46]. To ensure that \mathbf{E}^P , utilized by our mask classification decoder, contains robust and distinguishable local semantics, we incorporate deep supervision into $\mathbf{F}_{\frac{1}{4}}^F$. Specifically, we attach $\mathbf{F}_{\frac{1}{4}}^F$ with a lightweight fully convolutional decoder head and directly supervise this auxiliary network to produce semantic predictions. After two convolutional layers, the auxiliary semantic predictions with $(N - 1)$ channels and the same resolution as $\mathbf{F}_{\frac{1}{4}}^F$ are generated (excluding the ‘‘no object’’ category). This design enables the corresponding encoder layers to produce a $\mathbf{F}_{\frac{1}{4}}^F$ with more distinguishable local semantics, further ensuring that the pixel decoder can generate a more distinguishable \mathbf{E}^P , and ultimately leading to improved scene parsing performance without increasing network parameters or computational complexity.

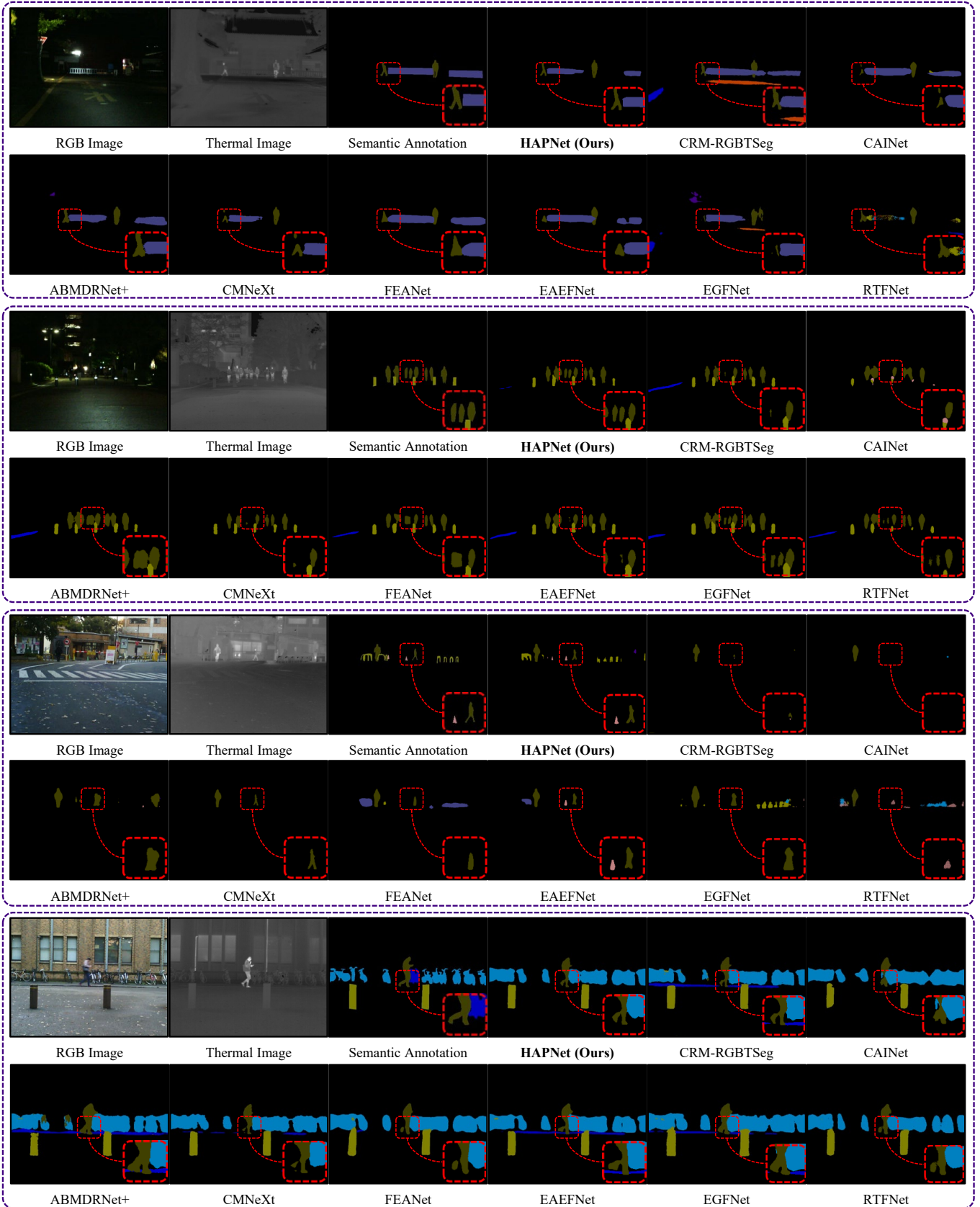


Fig. 2: Qualitative comparisons with the SoTA RGB-T scene parsing networks on the MFNet test set, where significantly improved regions are shown with red dashed boxes.

E. Loss Function

We use a combination of the pixel-wise cross-entropy (CE) loss \mathcal{L}_{cls} for class prediction, along with the binary CE loss \mathcal{L}_{bce} and the dice loss $\mathcal{L}_{\text{dice}}$ for mask prediction. For our local semantics enhancement task, we directly calculate the standard CE loss \mathcal{L}_{ce} over its semantic predictions. Therefore, the overall loss function can be expressed as follows:

$$\mathcal{L} = \lambda_{\text{bce}}\mathcal{L}_{\text{bce}} + \lambda_{\text{dice}}\mathcal{L}_{\text{dice}} + \lambda_{\text{cls}}\mathcal{L}_{\text{cls}} + \lambda_{\text{ce}}\mathcal{L}_{\text{ce}}. \quad (3)$$

Following [36], we set $\lambda_{\text{bce}} = 5.0$, $\lambda_{\text{dice}} = 5.0$, $\lambda_{\text{cls}} = 2.0$, and $\lambda_{\text{ce}} = 0.4$, respectively. Additionally, we employ bipartite matching [47] to determine the least-cost assignment during model training.

IV. EXPERIMENTS

We conduct extensive experiments in this article to evaluate the performance of our developed HAPNet both quantitatively and qualitatively. We further quantify the generalizability of HAPNet for RGB-depth/HHA (RGB-D/HHA) scene parsing. The following subsections provide details on the datasets and experimental setup, the evaluation metrics, as well as the comprehensive evaluation of our proposed method.

A. Datasets and Experimental Setup

We first compare HAPNet with other SoTA RGB-T scene parsing networks on the following three public datasets:

1) **MFNet** [5]: This is an urban driving scene parsing dataset. An InfReC R500 camera was utilized to capture 1,569 pairs of synchronized RGB and thermal images at a resolution of 640×480 pixels. The dataset provides semantic annotations of nine classes: bike, person, car, road lanes, guardrail, car stop, bump, color cone, and background. We adopt the same dataset splitting strategy as introduced in [5].

2) **PST900** [1]: This dataset contains 894 pairs of RGB and thermal images captured in challenging underground environments (originally released on the DARPA Subterranean Challenge). The RGB images were acquired using a Stereolabs ZED Mini stereo camera, while the thermal images were captured using a FLIR Boson 320 camera, both at a resolution of $1,280 \times 720$ pixels. The dataset has five categories of semantic annotations: background, fire extinguisher, backpack, hand drill, and survivor. We adopt the same data splitting strategy¹ as described in [1].

3) **KP Day-Night** [57]: This dataset contains 950 well-rectified RGB-T image pairs (resolution: 640×512 pixels) captured in urban driving scenes. This study [57] provides semantic annotations of 19 categories (identical to the CityScapes [58] dataset). We adopt the same data splitting strategy presented in [7] to train and evaluate our method.

Furthermore, we conduct an additional experiment on the NYU-Depth V2 dataset [59] to evaluate the generalizability of our network for RGB-D/HHA scene parsing.

4) **NYU-Depth V2** [59]: This dataset has been widely used for the evaluation of indoor scene parsing performance evaluation. It provides 1,449 pairs of RGB and depth images (resolution: 480×640 pixels), and semantic annotations for 40 categories. We adopt the same dataset splitting strategy as presented in [40].

B. Evaluation Metrics

We employ two widely used evaluation metrics: accuracy (Acc) and intersection over union (IoU), to quantify the scene parsing performance with respect to each category. The mean values of these two metrics across all categories (denoted as mIoU and mAcc, respectively) are also computed to quantify the comprehensive network performance.

C. Implementation Details

Our model was trained for 200 epochs on an NVIDIA RTX 3090 GPU, utilizing the AdamW optimizer [60] with an initial learning rate of 2×10^{-4} and a weight decay of 5×10^{-2} . Following the common practice employed in [16], we apply a layer-wise learning rate decay of 0.9 for our VFM encoder. For the experiments conducted on the NYU dataset, we employ RGB images and the HHA encoding of depth images as model input. We conduct all ablation studies on the widely utilized MFNet dataset, with the auxiliary task omitted to ensure training efficiency. The performance improvement (an increase in mIoU by 0.6%) between Sect. IV-D and Sect. IV-E demonstrate the effectiveness of the auxiliary task.

D. Comparisons with SoTA Scene Parsing Networks

We conduct quantitative comparisons with 12, 10, and four SoTA RGB-T scene parsing networks on the MFNet [5], PST900 [1], and KP Day-Night [57] datasets, respectively. The results are detailed in Tables I, III, and II, respectively. Additionally, we present the qualitative comparisons on these three datasets, as shown in Fig. 2, 3, and 4, respectively.

Specifically, our proposed HAPNet achieves the highest mIoU across all datasets, outperforming SoTA methods by 0.1-8.3% on the MFNet dataset, 1.0-32.0% on the PST900 dataset, and 2.4-28.9% on the KP day-night dataset, respectively. These results demonstrate the robustness and effectiveness of HAPNet for RGB-T scene parsing in various scenarios, ranging from complex urban driving scenes to challenging underground scenes. Notably, HAPNet outperforms CRM-RGBTseg [7], another SoTA Transformer-based approach based on the mask classification paradigm, demonstrating the efficacy of our adapter-based hybrid, asymmetric architecture in heterogeneous feature fusion. The qualitative results also demonstrate the superior capability of HAPNet in handling various scenes with challenging lighting conditions.

In addition, HAPNet demonstrates promising generalizability for RGB-D/HHA scene parsing. As shown in Table IV, our method outperforms all other RGB-T scene parsing networks on the NYU Depth V2 dataset. Specifically, HAPNet achieves an mIoU higher than ECGFNet [49] and RTFNet [4] by 3.5% and 5.9%, respectively. Meanwhile, these results suggest

¹The number of image pairs being published is fewer than what was reported in publication [1].

TABLE I: Quantitative comparisons (%) with the SoTA RGB-T scene parsing methods on the MFNet test set. The symbol ‘-’ denotes missing data in the original publication, and the best results are presented in bold font.

Methods	Car		Person		Bike		Curve		Car Stop		Guardrail		Color Cone		Bump		mAcc	mIoU
	Acc	IoU	Acc	IoU	Acc	IoU	Acc	IoU	Acc	IoU	Acc	IoU	Acc	IoU	Acc	IoU		
MFNet [5]	77.2	65.9	67.0	58.9	53.9	42.9	36.2	29.9	19.1	9.9	0.1	8.5	30.3	25.2	30.0	27.7	45.1	39.7
RTFNet [4]	93.0	87.4	79.3	70.3	76.8	62.7	60.7	45.3	38.5	29.8	0.0	0.0	45.5	29.1	74.7	55.7	63.1	53.2
FuseSeg [25]	93.1	87.9	81.4	71.7	78.5	64.6	68.4	44.8	29.1	22.7	63.7	6.4	55.8	46.9	66.4	47.9	70.6	54.5
EGFNet [48]	95.8	87.6	89.0	69.8	80.6	58.8	71.5	42.8	48.7	33.8	33.6	7.0	65.3	48.3	71.1	47.1	72.7	54.8
ABMDRNet [6]	94.3	84.8	90.0	69.6	75.7	60.3	64.0	45.1	44.1	33.1	31.0	5.1	61.7	47.4	66.2	50.0	69.5	54.8
ECGFNet [49]	89.4	83.5	85.2	72.1	72.9	61.6	62.8	40.5	44.8	30.8	45.2	11.1	57.2	49.7	65.1	50.9	69.1	55.3
FEANet [21]	93.3	87.8	82.7	71.1	76.7	61.1	65.5	46.5	26.6	22.1	70.8	6.6	66.6	55.3	77.3	48.9	73.2	55.3
ABMDRNet+ [20]	95.2	87.1	92.5	69.8	76.2	60.9	72.0	47.8	42.3	34.2	66.8	8.2	64.8	50.2	63.5	55.0	74.7	56.8
CAINet [10]	93.0	88.5	74.6	66.3	85.2	68.7	65.9	55.4	34.7	31.5	65.6	9.0	55.6	48.9	85.0	60.7	73.2	58.6
EAEFNet [3]	95.4	87.6	85.2	72.6	79.9	63.8	70.6	48.6	47.9	35.0	62.8	14.2	62.7	52.4	71.9	58.3	75.1	58.9
CMX [8]	-	90.1	-	75.2	-	64.5	-	50.2	-	35.3	-	8.5	-	54.2	-	60.6	-	59.7
CRM-RGBTSeg [7]	-	90.0	-	75.1	-	67.0	-	45.2	-	49.7	-	18.4	-	54.2	-	54.4	-	61.4
HAPNet (Ours)	95.1	90.6	85.5	75.4	79.0	67.2	67.9	51.1	59.5	48.4	16.0	4.2	65.0	59.1	80.3	59.1	98.3	61.5

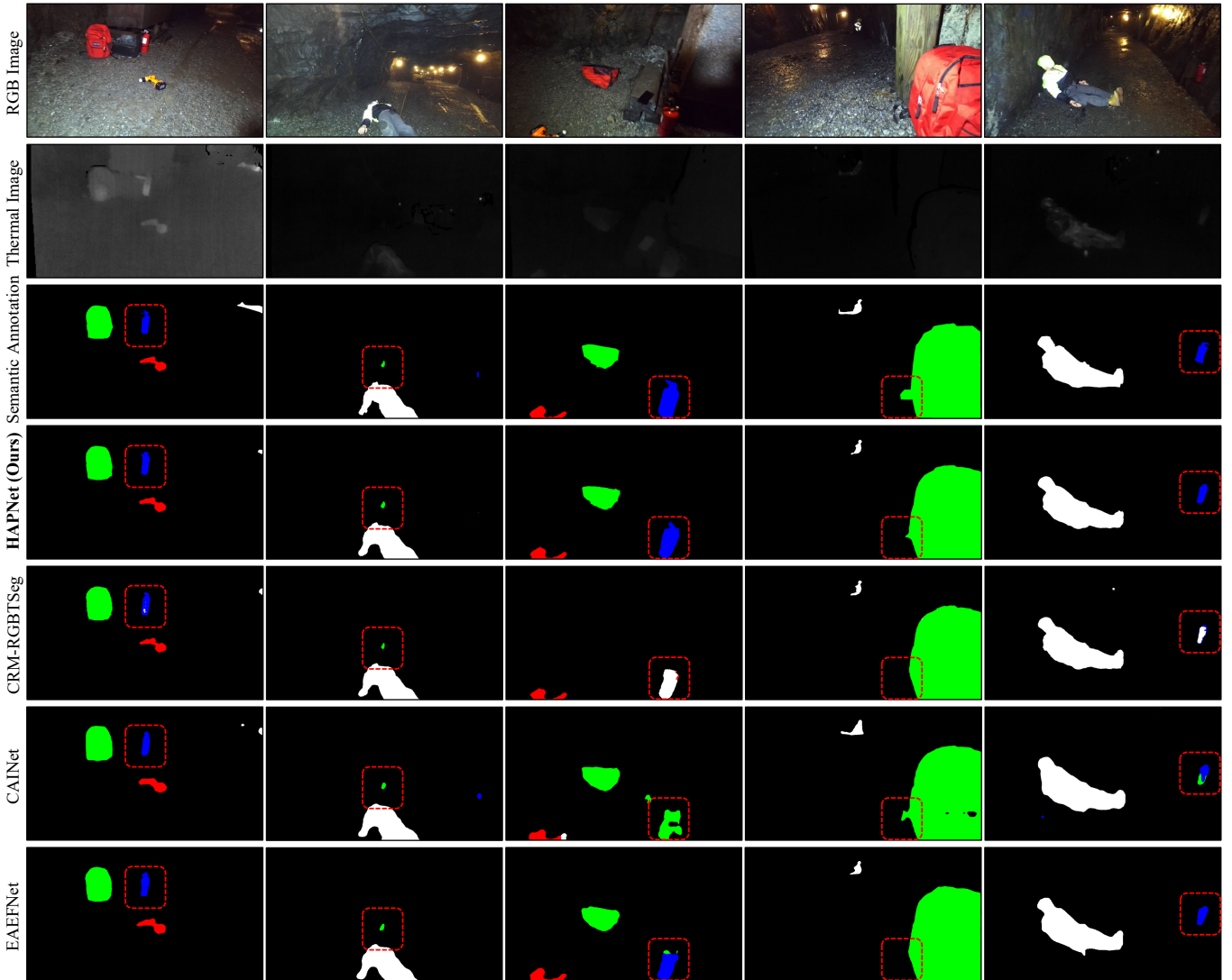


Fig. 3: Qualitative comparisons with the SoTA RGB-T scene parsing networks on the PST900 test set, where significantly improved regions are shown with red dashed boxes.

TABLE II: Quantitative comparisons (%) with the SoTA RGB-T scene parsing methods on the KP day-night test set. The best results are presented in bold font.

Methods	Road	Sidewalk	Building	Fence	Pole	Traffic light	Traffic sign	Vegetation	Terrain	Sky	Person	Rider	Car	Truck	Bus	Motorcycle	Bicycle	mIoU
MFNet [5]	93.5	23.6	75.1	0.1	9.1	0.0	0.0	69.3	0.2	90.4	24.0	0.0	69.6	0.3	0.3	0.0	0.6	24.0
RTFNet [4]	94.6	39.4	86.6	0.6	0.0	0.0	0.0	81.7	3.7	92.8	58.4	0.0	87.7	0.0	0.0	0.0	0.5	28.7
CMX [8]	97.7	53.8	90.2	47.1	46.2	10.9	45.1	87.2	34.3	93.5	74.5	0.0	91.6	0.0	59.7	46.1	0.2	46.2
CRM-RGBTSeg [7]	99.0	61.9	91.8	58.7	50.6	39.2	55.3	89.2	23.2	94.3	85.2	2.9	95.3	0.0	80.5	66.2	54.6	55.2
HAPNet (Ours)	98.6	59.3	91.5	57.0	58.0	41.0	56.8	87.8	30.4	94.8	81.8	21.3	94.2	0.0	69.7	49.9	43.8	57.6

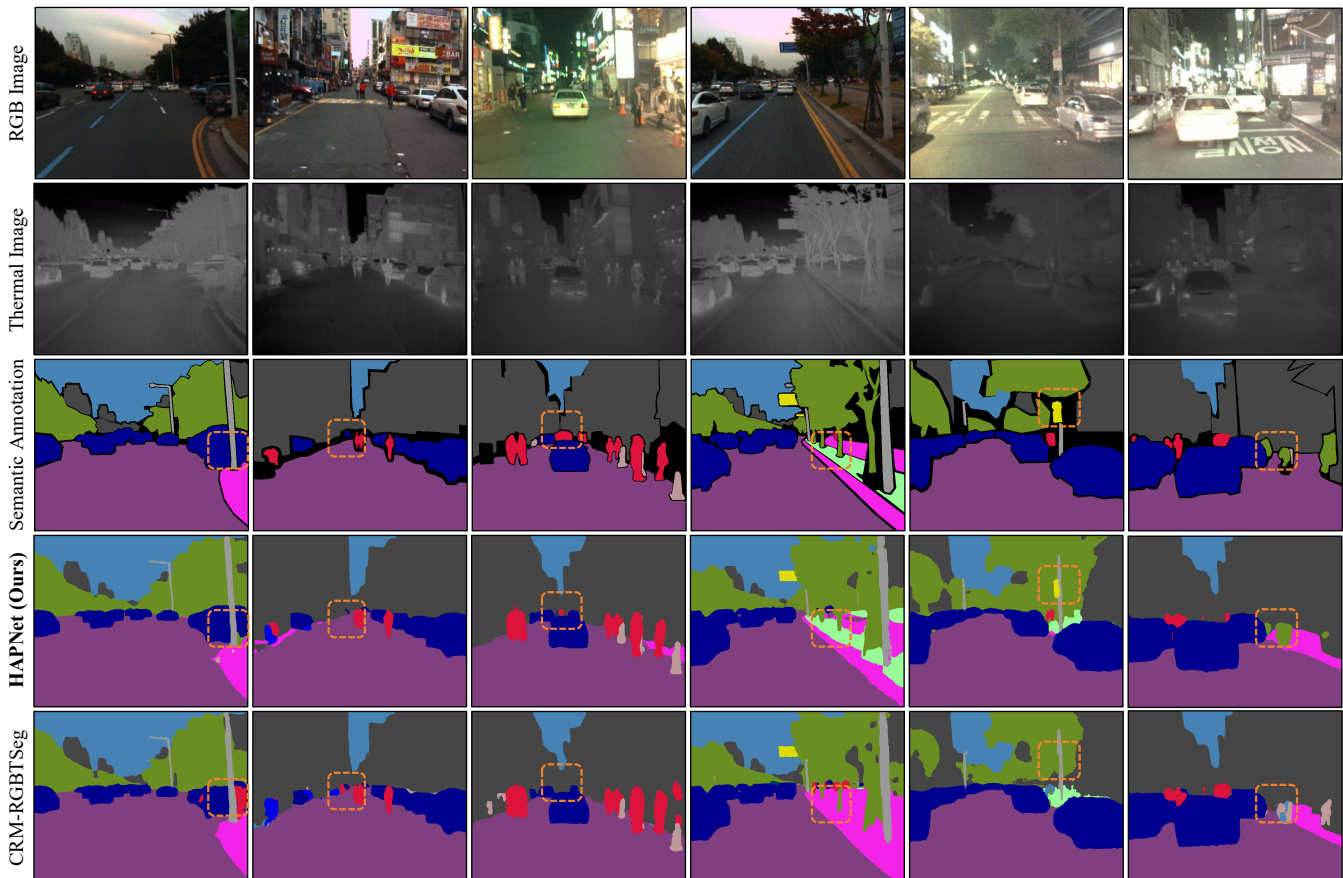


Fig. 4: Qualitative comparisons with the SoTA RGB-T scene parsing networks on the KP Day-Night test set, where significantly improved regions are shown with orange dashed boxes.

that HAPNet still lags behind SoTA methods, developed specifically for RGB-D/HHA data fusion, including Omnivore [51], DFormer-L [40], and OmniVec [50] (mIoU is lower by 2.2-5.8%). Additionally, it underperforms CMX [8], a SoTA general multi-modal data-fusion method by 1.9% on mIoU. We hypothesize that this performance gap stems from the inherently different data distributions between the thermal and depth/HHA modalities, which limits the applicability of our architecture in the RGB-D/HHA scene parsing domain.

E. Ablation Study

We first explore the performance of RGB-T scene parsing with respect to different input data combination strategies.

Given the asymmetric two-branch architecture, the RGB-T data can be fed into our HAPNet using nine different strategies to the VFM and CSPD, respectively, as shown in Table V. Among them, strategies E and I can be considered as single-modal versions (only RGB or thermal images are encoded by the network), yielding mIoU scores of only 53.9% and 51.5%, respectively. On the other hand, strategies A-D, and F-H, which employ both RGB and thermal images, achieve superior performance, validating the importance of modality complementation. Notably, strategy D, employing RGB images as inputs to the VFM branch while using a combination of RGB-T data in the CSPD, achieves the highest mIoU of 60.9%. This result demonstrates that encoding thermal images using the VFM may deteriorate features and degrade the overall

TABLE III: Quantitative comparisons (%) with the SoTA RGB-T scene parsing methods on the PST900 test set. The symbol “-” denotes missing data in the original publication, and the best results are presented in bold font.

Methods	Background		Fire-Extinguisher		Backpack		Hand-Drill		Survivor		mAcc	mIoU
	Acc	IoU	Acc	IoU	Acc	IoU	Acc	IoU	Acc	IoU		
MFNet [5]	-	98.6	-	41.1	-	64.2	-	60.3	-	20.7	-	57.0
RTFNet [4]	-	98.9	-	36.4	-	75.3	-	52.0	-	25.3	-	57.6
EGFNet [48]	-	99.2	-	74.3	-	83.0	-	71.2	-	64.6	-	78.5
ABMDRNet [6]	-	98.7	-	24.1	-	72.9	-	54.9	-	57.6	-	67.3
FEANet [21]	-	-	-	-	-	-	-	-	-	-	91.4	85.5
DBCNet [2]	-	98.9	-	62.3	-	71.1	-	52.4	-	40.6	-	74.5
CAINet [10]	99.6	99.5	95.8	80.3	96.0	88.0	88.3	77.2	91.3	78.6	94.2	84.7
EAEFNet [3]	99.8	99.5	92.2	80.4	91.0	87.7	93.0	83.9	79.3	75.6	91.1	85.4
GMNet [9]	99.8	99.4	90.2	85.1	89.0	83.8	88.2	73.7	80.8	78.3	89.6	84.1
CRM-RGBTseg [7]	-	99.6	-	79.5	-	89.6	-	89.0	-	82.2	-	88.0
HAPNet (Ours)	99.8	99.6	93.9	81.3	95.1	92.0	95.5	89.3	85.6	82.4	94.0	89.0

TABLE IV: Quantitative comparisons (%) with the SoTA data-fusion scene parsing networks on the NYU-Depth V2 test set.

Input Data	Methods	Pixel Acc	mAcc	mIoU	Rank
RGB-D	OmniVec [50]	-	-	60.8	1
	Omnivore [51]	-	-	56.8	8
	TokenFusion [52]	79.0	66.9	54.2	16
	DFormer-L [40]	-	-	57.2	5
	AsymFormer [53]	78.5	-	54.1	17
	RTFNet [4]	-	64.8	49.1	59
	ECGFNet [49]	-	65.2	51.5	37
RGB-HHA	CMX [8]	-	-	56.9	6
	SA-Gate [54]	-	-	52.4	31
	HAPNet (Ours)	79.2	68.8	55.0	15

performance, which verifies our hypothesis stated in Sect. I.

Our CSPD extracts multi-scale spatial priors from both RGB and thermal images, which are subsequently fused with the VFM context features to implicitly enrich the local semantics. To further explore the most suitable structure for the CSPD, we replace the basic ConvNeXt blocks with other mainstream hierarchical encoder structures, as illustrated in Table VI. Compared to the early ResNet and the latest Swin-Transformer, ConvNeXt exhibits superior performance (yielding an mIoU of 60.9%).

In addition, we investigate the impact of employing separate weights for the two modalities, and this strategy yields a slightly better result. However, considering the trade-off between accuracy and model complexity, we still adopt the weight-sharing strategy, as the weight-separating strategy only achieves an improvement of 0.3% in terms of mIoU while incurring a substantial increase in the modal parameters.

Furthermore, we evaluate the effectiveness of GLCA and CCG. As presented in Table VII, removing either of them leads to a significant performance deterioration of HAPNet. The baseline setup, which could only perform cross-modal feature fusion via element-wise summation between spatial priors and global context, exhibits a 3.0% lower mIoU compared to the complete HAPNet.

To validate the effectiveness of our proposed asymmetric architecture, we first construct baseline architectures incorporating symmetric duplex encoders based on BEiTv2 [17] and ConvNeXt [14], respectively. As shown in Table VIII, such baseline architectures fail to achieve performance comparable to that of our developed HAPNet. Specifically, the duplex, symmetric ConvNeXt and BEiTv2 architectures fall short of HAPNet, with a decrease in mIoU by 3.5-2.4% and 27.2-25.9%, respectively. These findings lend further support to our hypothesis stated in Sect. I, suggesting that applying asymmetric architectures to RGB and thermal modalities can play to their own strengths. Importantly, the disappointing performance of the symmetric duplex BEiTv2 encoder suggests that directly applying VFMs for the RGB-T scene parsing task might not be suitable.

Moreover, we also evaluate the compatibility of HAPNet with various SoTA VFMs, including those trained through traditional supervised learning (DeiT [55] and AugReg [56]) as well as the most recent models developed based on self-supervised pre-training (BEiT [16], BEiTv2 [17], and DINOv2 [18]). As shown in Table IX, BEiTv2 achieves the highest mIoU at 60.9%, outperforming all other models on the RGB-T scene parsing task. Given BEiTv2’s superior performance, we empirically determine it to be the most suitable VFM for this task, thereby adopting BEiTv2 as the default VFM within HAPNet.

V. CONCLUSION AND FUTURE WORK

In this article, we revisited the design of heterogeneous feature extraction and fusion strategies. Drawing upon the inherent characteristics of RGB and thermal data, we developed a novel hybrid, asymmetric network to capitalize on their unique strengths, leveraging the powerful VFM for this specific task. We first developed a cross-modal spatial prior descriptor to capture local semantics jointly from RGB-T data. Additionally, we designed a progressive heterogeneous feature integrator, consisting of a global-local context aggregator and a complementary context generator, to fuse heterogeneous features more effectively. We also introduced an auxiliary task to further enhance the local semantics of the fused features,

TABLE V: An ablation study (%) on different data input strategies on the MFNet test set.

Strategies	VFM	CSPD	Car	Person	Bike	Curve	Car Stop	Guardrail	Color Cone	Bump	mAcc	mIoU
			IoU	IoU	IoU	IoU	IoU	IoU	IoU	IoU		
A	RGB + T	RGB + T	89.3	73.9	66.1	48.0	32.4	4.4	55.7	62.6	74.3	58.9
B	RGB + T	RGB	88.3	69.1	64.3	44.3	32.3	4.3	52.9	44.5	67.0	55.3
C	RGB + T	Thermal	85.5	72.7	54.6	39.3	28.5	8.2	46.1	55.4	71.5	54.2
D (Ours)	RGB	RGB + T	89.1	76.0	67.2	50.6	41.3	7.9	58.6	58.7	75.1	60.9
E	RGB	RGB	87.9	62.5	63.8	40.7	28.2	5.6	52.1	47.1	66.7	53.9
F	RGB	Thermal	86.7	73.9	60.3	39.1	33.0	7.3	53.6	59.0	74.6	56.7
G	Thermal	RGB + T	89.6	74.6	65.1	48.9	33.9	1.5	53.9	56.8	68.8	58.1
H	Thermal	RGB	88.4	69.3	65.3	43.2	29.7	4.4	53.4	44.4	67.4	55.1
I	Thermal	Thermal	84.5	71.8	53.8	35.0	24.3	3.8	38.4	54.5	66.6	51.5

TABLE VI: An ablation study (%) on different CSPD construction blocks on the MFNet test set.

Encoders	Car	Person	Bike	Curve	Car Stop	Guardrail	Color Cone	Bump	mAcc	mIoU
	IoU	IoU	IoU	IoU	IoU	IoU	IoU	IoU		
Duplex ResNet sharing weights	66.3	48.0	38.4	19.9	9.1	0.0	29.6	23.6	42.3	36.8
Duplex Swin-Transformer sharing weights	89.7	74.1	67.2	47.6	31.0	6.3	52.7	57.0	74.6	58.2
Duplex ConvNeXt with separate weights	89.6	74.6	66.6	46.3	45.7	10.2	56.6	62.5	73.6	61.2
Duplex ConvNeXt sharing weights (Ours)	89.1	76.0	67.2	50.6	41.3	7.9	58.6	58.7	75.1	60.9

TABLE VII: An ablation study (%) on the effectiveness of GLCA and CCG on the MFNet test set. When both components are removed, the spatial priors extracted using CSPD and the global context extracted using ViT are fused via element-wise summation after resolution alignment.

GLCA	CCG	Fusion Strategies	Car	Person	Bike	Curve	Car Stop	Guardrail	Color Cone	Bump	mAcc	mIoU
			IoU	IoU	IoU	IoU	IoU	IoU	IoU	IoU		
		Element-wise Summation	89.2	73.5	65.7	50.0	33.0	4.1	52.0	55.4	71.1	57.9
✓		Local Semantics Enhanced	89.9	74.7	67.0	50.0	37.0	5.8	52.9	55.9	72.9	59.1
	✓	Global Context Updated	89.6	74.5	67.0	46.6	36.9	2.9	53.3	53.3	72.4	58.0
✓	✓	Both (Ours)	89.1	76.0	67.2	50.6	41.3	7.9	58.6	58.7	75.1	60.9

TABLE VIII: An ablation study (%) on different duplex encoder architectures on the MFNet test set.

Methods	Car	Person	Bike	Curve	Car Stop	Guardrail	Color Cone	Bump	mAcc	mIoU
	IoU	IoU	IoU	IoU	IoU	IoU	IoU	IoU		
Duplex BEiTv2 concatenation	65.7	57.4	12.7	27.7	8.5	0.0	14.7	20.6	40.9	33.7
Duplex BEiTv2 summation	65.4	57.1	23.3	28.0	8.5	0.0	19.9	16.2	42.6	35.0
Duplex ConvNeXt concatenation	89.7	74.1	66.4	45.3	29.8	4.8	52.8	55.5	69.2	57.4
Duplex ConvNeXt summation	90.7	74.6	66.9	46.8	32.9	6.6	56.6	52.7	72.0	58.5
HAPNet (Ours)	89.1	76.0	67.2	50.6	41.3	7.9	58.6	58.7	75.1	60.9

TABLE IX: An ablation study (%) on different VFMs on the MFNet test set. “MM” represents multi-modal pre-training. BEiT and BEiTv2 are trained via a self-supervised learning strategy named masked image modeling, while DINOv2 is trained via discriminative self-supervised learning strategy.

VFM	Pre-training Strategy	Dataset	Car	Person	Bike	Curve	Car Stop	Guardrail	Color Cone	Bump	mAcc	mIoU
			IoU	IoU	IoU	IoU	IoU	IoU	IoU	IoU		
DeiT [55]	Supervised	ImageNet-1K	90.4	75.2	66.6	47.6	36.3	0.7	59.9	60.0	68.3	59.4
AugReg [56]	Supervised	ImageNet-22K	90.3	74.9	66.8	48.2	35.8	6.0	56.6	56.5	74.7	59.3
BEiT [16]	Self-Supervised	ImageNet-22K	90.7	75.0	67.6	48.6	39.1	4.2	55.0	59.0	72.5	59.7
DINOv2 [18]	Self-Supervised	LVD-142M (MM) [18]	90.0	74.7	66.8	45.1	42.1	9.7	56.2	59.7	76.4	60.3
BEiTv2 [17]	Self-Supervised	ImageNet-22K (MM)	89.1	76.0	67.2	50.6	41.3	7.9	58.6	58.7	75.1	60.9

leading to improved overall performance. Extensive experiments demonstrate that HAPNet not only achieves the state-of-the-art performance for RGB-T scene parsing across three public datasets but also shows great potential to generalize well for RGB-HHA scene parsing in indoor scenarios. Despite its superior performance over other existing approaches, the generalizability of HAPNet for RGB-X (where “X” represents, but is not limited to, depth, surface normal, and so forth) can be further improved. Additionally, considering scene parsing is a common functionality embedded in autonomous cars, mobile robots, and drones, the real-time performance of HAPNet is crucial, which is also a direction for possible future work.

REFERENCES

- [1] S. S. Shivakumar *et al.*, “PST900: RGB-Thermal Calibration, Dataset and Segmentation Network,” in *2020 IEEE International Conference on Robotics and Automation (ICRA)*. IEEE, 2020, pp. 9441–9447.
- [2] W. Zhou *et al.*, “DBCNet: Dynamic Bilateral Cross-Fusion Network for RGB-T Urban Scene Understanding in Intelligent Vehicles,” *IEEE Transactions on Systems, Man, and Cybernetics: Systems*, vol. 53, no. 12, pp. 7631–7641, 2023.
- [3] M. Liang *et al.*, “Explicit Attention-Enhanced Fusion for RGB-Thermal Perception Tasks,” *IEEE Robotics and Automation Letters*, vol. 8, no. 7, pp. 4060–4067, 2023.
- [4] Y. Sun *et al.*, “RTFNet: RGB-Thermal Fusion Network for Semantic Segmentation of Urban Scenes,” *IEEE Robotics and Automation Letters*, vol. 4, no. 3, pp. 2576–2583, 2019.
- [5] Q. Ha *et al.*, “MFNet: Towards Real-Time Semantic Segmentation for Autonomous Vehicles with Multi-Spectral Scenes,” in *2017 IEEE/RSJ International Conference on Intelligent Robots and Systems (IROS)*. IEEE, 2017, pp. 5108–5115.
- [6] Q. Zhang *et al.*, “ABMDRNet: Adaptive-weighted Bi-directional Modality Difference Reduction Network for RGB-T Semantic Segmentation,” in *Proceedings of the IEEE/CVF Conference on Computer Vision and Pattern Recognition (CVPR)*, 2021, pp. 2633–2642.
- [7] U. Shin *et al.*, “Complementary Random Masking for RGB-Thermal Semantic Segmentation,” *arXiv preprint arXiv:2303.17386*, 2023.
- [8] J. Zhang *et al.*, “CMX: Cross-Modal Fusion for RGB-X Semantic Segmentation with Transformers,” *IEEE Transactions on Intelligent Transportation Systems*, vol. 24, no. 12, pp. 14 679–14 694, 2023.
- [9] W. Zhou *et al.*, “GMNet: Graded-Feature Multilabel-Learning Network for RGB-Thermal Urban Scene Semantic Segmentation,” *IEEE Transactions on Image Processing*, vol. 30, pp. 7790–7802, 2021.
- [10] Y. Lv *et al.*, “Context-Aware Interaction Network for RGB-T Semantic Segmentation,” *IEEE Transactions on Multimedia*, 2024, DOI:10.1109/TMM.2023.3349072.
- [11] W. Zhou *et al.*, “CACFNet: Cross-Modal Attention Cascaded Fusion Network for RGB-T Urban Scene Parsing,” *IEEE Transactions on Intelligent Vehicles*, vol. 9, no. 1, pp. 1919–1929, 2023.
- [12] K. He *et al.*, “Deep Residual Learning for Image Recognition,” in *Proceedings of the IEEE Conference on Computer Vision and Pattern Recognition (CVPR)*, 2016, pp. 770–778.
- [13] Z. Liu *et al.*, “Swin Transformer: Hierarchical Vision Transformer using Shifted Windows,” in *Proceedings of the IEEE/CVF International Conference on Computer Vision (ICCV)*, 2021, pp. 10 012–10 022.
- [14] Z. Liu *et al.*, “A ConvNet for the 2020s,” in *Proceedings of the IEEE/CVF Conference on Computer Vision and Pattern Recognition (CVPR)*, 2022, pp. 11 976–11 986.
- [15] Y. Feng *et al.*, “SNE-RoadSegV2: Advancing Heterogeneous Feature Fusion and Fallibility Awareness for Freespace Detection,” *arXiv preprint arXiv:2402.18918*, 2024.
- [16] H. Bao *et al.*, “BEiT: BERT Pre-Training of Image Transformers,” *arXiv preprint arXiv:2106.08254*, 2021.
- [17] Z. Peng *et al.*, “BEiT v2: Masked Image Modeling With Vector-Quantized Visual Tokenizers,” *arXiv preprint arXiv:2208.06366*, 2022.
- [18] M. Oquab *et al.*, “DINOv2: Learning Robust Visual Features Without Supervision,” *Transactions on Machine Learning Research*, 2023.
- [19] A. Krizhevsky *et al.*, “ImageNet Classification with Deep Convolutional Neural Networks,” *Advances in Neural Information Processing Systems (NeurIPS)*, vol. 25, pp. 1097–1105, 2012.
- [20] S. Zhao *et al.*, “Mitigating Modality Discrepancies for RGB-T Semantic Segmentation,” *IEEE Transactions on Neural Networks and Learning Systems*, 2023, DOI:10.1109/TNNLS.2022.3233089.
- [21] F. Deng *et al.*, “FEANet: Feature-Enhanced Attention Network for RGB-Thermal Real-time Semantic Segmentation,” in *2021 IEEE/RSJ International Conference on Intelligent Robots and Systems (IROS)*. IEEE, 2021, pp. 4467–4473.
- [22] J. Liu *et al.*, “Revisiting Modality-Specific Feature Compensation for Visible-Infrared Person Re-Identification,” *IEEE Transactions on Circuits and Systems for Video Technology*, vol. 32, no. 10, pp. 7226–7240, 2022.
- [23] D. Seichter *et al.*, “Efficient RGB-D Semantic Segmentation for Indoor Scene Analysis,” in *2021 IEEE International Conference on Robotics and Automation (ICRA)*. IEEE, 2021, pp. 13 525–13 531.
- [24] W. Zhou *et al.*, “MTANet: Multitask-Aware Network With Hierarchical Multimodal Fusion for RGB-T Urban Scene Understanding,” *IEEE Transactions on Intelligent Vehicles*, vol. 8, no. 1, pp. 48–58, 2022.
- [25] Y. Sun *et al.*, “FuseSeg: Semantic Segmentation of Urban Scenes Based on RGB and Thermal Data Fusion,” *IEEE Transactions on Automation Science and Engineering*, vol. 18, no. 3, pp. 1000–1011, 2020.
- [26] J. Long *et al.*, “Fully Convolutional Networks for Semantic Segmentation,” in *Proceedings of the IEEE/CVF Conference on Computer Vision and Pattern Recognition (CVPR)*, 2015, pp. 3431–3440.
- [27] L.-C. Chen *et al.*, “DeepLab: Semantic Image Segmentation with Deep Convolutional Nets, Atrous Convolution, and Fully Connected CRFs,” *IEEE Transactions on Pattern Analysis and Machine Intelligence*, vol. 40, no. 4, pp. 834–848, 2017.
- [28] L. Chen *et al.*, “Encoder-Decoder with Atrous Separable Convolution for Semantic Image Segmentation,” in *Proceedings of the European Conference on Computer Vision (ECCV)*, 2018, pp. 801–818.
- [29] T.-Y. Lin *et al.*, “Feature Pyramid Networks for Object Detection,” in *Proceedings of the IEEE/CVF Conference on Computer Vision and Pattern Recognition (CVPR)*, 2017, pp. 2117–2125.
- [30] A. Vaswani *et al.*, “Attention is All you Need,” *Advances in Neural Information Processing Systems (NeurIPS)*, vol. 30, pp. 5998–6008, 2017.
- [31] S. Zheng *et al.*, “Rethinking Semantic Segmentation From a Sequence-to-Sequence Perspective With Transformers,” in *Proceedings of the IEEE/CVF Conference on Computer Vision and Pattern Recognition (CVPR)*, 2021, pp. 6881–6890.
- [32] E. Xie *et al.*, “SegFormer: Simple and Efficient Design for Semantic Segmentation with Transformers,” *Advances in Neural Information Processing Systems (NeurIPS)*, vol. 34, pp. 12 077–12 090, 2021.
- [33] J. Dai *et al.*, “Convolutional Feature Masking for Joint Object and Stuff Segmentation,” in *Proceedings of the IEEE/CVF Conference on Computer Vision and Pattern Recognition (CVPR)*, 2015, pp. 3992–4000.
- [34] B. Hariharan *et al.*, “Simultaneous Detection and Segmentation,” in *Proceedings of the European Conference on Computer Vision (ECCV)*. Springer, 2014, pp. 297–312.
- [35] B. Cheng *et al.*, “Per-Pixel Classification is Not All You Need for Semantic Segmentation,” *Advances in Neural Information Processing Systems (NeurIPS)*, vol. 34, pp. 17 864–17 875, 2021.
- [36] B. Cheng *et al.*, “Masked-attention Mask Transformer for Universal Image Segmentation,” in *Proceedings of the IEEE/CVF Conference on Computer Vision and Pattern Recognition (CVPR)*, 2022, pp. 1290–1299.
- [37] G. Huang *et al.*, “Densely Connected Convolutional Networks,” in *Proceedings of the IEEE Conference on Computer Vision and Pattern Recognition (CVPR)*, 2017, pp. 4700–4708.
- [38] K. He *et al.*, “Masked Autoencoders Are Scalable Vision Learners,” in *Proceedings of the IEEE/CVF Conference on Computer Vision and Pattern Recognition (CVPR)*, 2022, pp. 16 000–16 009.
- [39] T. Xiao *et al.*, “Unified Perceptual Parsing for Scene Understanding,” in *Proceedings of the European Conference on Computer Vision (ECCV)*, 2018, pp. 418–434.
- [40] B. Yin *et al.*, “DFormer: Rethinking RGBD Representation Learning for Semantic Segmentation,” *International Conference on Learning Representations (ICLR)*, 2024.
- [41] K. Li *et al.*, “UniFormer: Unifying Convolution and Self-Attention for Visual Recognition,” *IEEE Transactions on Pattern Analysis and Machine Intelligence*, vol. 45, no. 10, pp. 12 581–12 600, 2023.
- [42] S. Xie *et al.*, “Aggregated Residual Transformations for Deep Neural Networks,” in *Proceedings of the IEEE Conference on Computer Vision and Pattern Recognition (CVPR)*, 2017, pp. 1492–1500.

- [43] J. Li *et al.*, “RoadFormer: Duplex Transformer for RGB-Normal Semantic Road Scene Parsing,” *arXiv preprint arXiv:2309.10356*, 2024, to be published by IEEE Transactions on Intelligent Vehicles.
- [44] R. Bachmann *et al.*, “MultiMAE: Multi-modal Multi-task Masked Autoencoders,” in *European Conference on Computer Vision (ECCV)*. Springer, 2022, pp. 348–367.
- [45] S. Huang *et al.*, “FaPN: Feature-Aligned Pyramid Network for Dense Image Prediction,” in *Proceedings of the IEEE/CVF International Conference on Computer Vision (ICCV)*, 2021, pp. 864–873.
- [46] X. Yang *et al.*, “PolyMaX: General Dense Prediction with Mask Transformer,” in *Proceedings of the IEEE/CVF Winter Conference on Applications of Computer Vision (WACV)*, 2024, pp. 1050–1061.
- [47] N. Carion *et al.*, “End-to-End Object Detection with Transformers,” in *European Conference on Computer Vision (ECCV)*. Springer, 2020, pp. 213–229.
- [48] W. Zhou *et al.*, “Edge-Aware Guidance Fusion Network for RGB–Thermal Scene Parsing,” in *Proceedings of the AAAI Conference on Artificial Intelligence*, vol. 36, no. 3, 2022, pp. 3571–3579.
- [49] W. Zhou *et al.*, “Embedded Control Gate Fusion and Attention Residual Learning for RGB–Thermal Urban Scene Parsing,” *IEEE Transactions on Intelligent Transportation Systems*, vol. 24, no. 5, pp. 4794–4803, 2023.
- [50] S. Srivastava and G. Sharma, “OmniVec: Learning Robust Representations With Cross Modal Sharing,” in *Proceedings of the IEEE/CVF Winter Conference on Applications of Computer Vision (WACV)*, 2024, pp. 1236–1248.
- [51] R. Girdhar *et al.*, “OMNIVORE: A Single Model for Many Visual Modalities,” in *Proceedings of the IEEE/CVF Conference on Computer Vision and Pattern Recognition (CVPR)*, 2022, pp. 16 102–16 112.
- [52] Y. Wang *et al.*, “Multimodal Token Fusion for Vision Transformers,” in *Proceedings of the IEEE/CVF Conference on Computer Vision and Pattern Recognition (CVPR)*, 2022, pp. 12 186–12 195.
- [53] S. Du *et al.*, “AsymFormer: Asymmetrical Cross-Modal Representation Learning for Mobile Platform Real-Time RGB-D Semantic Segmentation,” *arXiv preprint arXiv:2309.14065*, 2023.
- [54] X. Chen *et al.*, “Bi-directional Cross-Modality Feature Propagation with Separation-and-Aggregation Gate for RGB-D Semantic Segmentation,” in *European Conference on Computer Vision (ECCV)*. Springer, 2020, pp. 561–577.
- [55] H. Touvron *et al.*, “Training data-efficient image transformers & distillation through attention,” in *International Conference on Machine Learning (ICML)*. PMLR, 2021, pp. 10 347–10 357.
- [56] A. P. Steiner *et al.*, “How to train your ViT? Data, Augmentation, and Regularization in Vision Transformers,” *Transactions on Machine Learning Research*, 2022.
- [57] Y.-H. Kim *et al.*, “MS-UDA: Multi-Spectral Unsupervised Domain Adaptation for Thermal Image Semantic Segmentation,” *IEEE Robotics and Automation Letters*, vol. 6, no. 4, pp. 6497–6504, 2021.
- [58] M. Cordts *et al.*, “The Cityscapes Dataset for Semantic Urban Scene Understanding,” in *Proceedings of the IEEE/CVF Conference on Computer Vision and Pattern Recognition (CVPR)*, 2016, pp. 3213–3223.
- [59] N. Silberman *et al.*, “Indoor Segmentation and Support Inference from RGBD Images,” in *European Conference on Computer Vision (ECCV)*. Springer, 2012, pp. 746–760.
- [60] I. Loshchilov and F. Hutter, “Decoupled Weight Decay Regularization,” in *International Conference on Learning Representations (ICLR)*, 2018.